Contributions to Mineralogy and Petrology (2026) 181:12
https://doi.org/10.1007/s00410-025-02294-6

ORIGINAL PAPER

Revised PVT equations of state for almandine and spessartine garnets: implications for piezobarometry

Ross J. Angel[1] · Marta Morana[2] · Sergio Speziale[3] · Nicola P. M. Casati[4] · Alan B. Woodland[5] · Matteo Alvaro[6] · Guy L. Hovis[7] · Mario Tribaudino[8]

Received: 30 September 2025 / Accepted: 19 December 2025 / Published online: 29 January 2026
© The Author(s), under exclusive licence to Springer-Verlag GmbH Germany, part of Springer Nature 2026

Abstract

Previously published thermal expansion data for almandine and spessartine garnets are sparse and inconsistent. We have therefore measured the thermal expansion of two garnets of compositions Alm90 Grs2.7 Py2.3 Ski4.5 (sample Alm90) and Sps81 Alm15 Grs3 And1 (sample Sps81) from ca. 90 K to ca. 780 K by synchrotron X-ray powder diffraction using quartz as an internal calibrant for temperature. The adiabatic elastic tensors of these two samples have been determined by single-crystal Brillouin scattering at room conditions; for the Alm90 sample c_{11} = 302.0(5), c_{12} = 111.3(4), c_{44} = 93.3(1), giving K_S = 174.9(4) GPa, and for the Sps81 sample c_{11} = 303.1(4), c_{12} = 109.5(4), c_{44} = 93.6(2), giving K_S = 174.0(4) GPa. These new data have been used in combination with P-V, P-T-V and P-T-Ks data from the literature to determine the equations of state (EoS) of end-member almandine and spessartine. The parameters of *q*-compromise Mie-Grüneisen-Debye thermal pressure EoS with a third-order Birch-Murnaghan EoS to describe the compressional properties at room temperature are:

	Almandine	Spessartine
V_0: cm^3/mol	115.25	117.92
K_{0T}: GPa	174.1(4)	172.2(7)
K_0'	5.56(14)	5.6(3)
θ_D: K	549(4)	569(5)
γ_0	1.186(4)	1.135(6)
K_{0S}: GPa	175.6(4)	173.5(7)

The parameters are available in .eos files for the EosFit suite of programs in the supplementary data, and from www.rossangel.com and www.mineralogylab.com. The most significant changes from the previous EoS are the lower Debye temperatures because our data show higher thermal expansion above room temperature. The biggest consequence for host-inclusion piezobarometry is that these new EoS lead to lower entrapment temperatures for zircon inclusions in garnet. We also show that there is no significant difference in the P-V/V_0 behaviour of almandine and spessartine and that the available experimental data for intermediate compositions does not indicate any significant non-ideality in the compressional or thermal expansion behaviour of almandine-spessartine garnets.

Keywords Almandine · Spessartine · Elasticity · Thermal expansion · Equation of state

Communicated by Dante Canil.

Extended author information available on the last page of the article

Introduction

Garnets are common minerals in metamorphic rocks and commonly trap other minerals as inclusions as they grow. The measurement of the stress and strain state of such inclusions can be used, if the equations of state (EoS) of both host and inclusion are known, to determine the P and T conditions of garnet growth (e.g. Angel et al. 2017b; Kohn et al. 2023) or in some cases the conditions at which resetting occurred (e.g. Campomenosi et al. 2023; Zhong et al. 2024). Both cases provide constraints on the P-T histories of garnet-containing rocks that are independent of conventional chemical thermobarometry based on equilibrium thermodynamics. Further, partial resetting of inclusion stress states during exhumation can be used to infer exhumation rates (e.g. Zhong et al. 2018). All of these applications require accurate and precise EoS that describe the variation of the volumes and bulk modulus of both the host and inclusion mineral as a function of P and T.

However, the review by Angel et al. (2022) showed that thermal expansion data for both almandine and spessartine garnets were both sparse and inconsistent. Therefore, several arbitrary assumptions and decisions had to be made about the choice of datasets to use to obtain a P-T-V EoS for both of these garnet endmembers. This made the EoS published by Angel et al. (2022) for almandine and spessartine provisional and uncertain, in stark contrast to the very well constrained EoS for grossular and pyrope.

We have now resolved this issue by collecting X-ray diffraction data from 90 to ca. 780 K for two natural garnet samples, one almandine-rich and one spessartine-rich, along with Brillouin scattering data at room conditions to determine their elastic tensors and bulk moduli. We show that the variation of thermal expansion and compressibility across the almandine-spessartine join is sufficiently small that the data from these samples can be combined with those from endmembers to provide well-constrained EoS for both endmember compositions. These can then be used to calculate the variation of the volumes and bulk moduli for intermediate compositions. The implications of these new EoS for host-inclusion piezobarometry involving almandine-spessartine hosts are discussed.

Experimental

Samples

The almandine is sample FRA-1 of Woodland et al. (1995) and comes from a metamorphic complex near Collobrieres, southern France. Mossbauer analysis showed that some skiagite ($Fe_3^{2+}Fe_2^{3+}Si_3O_{12}$) component is present; the composition determined by combining Mossbauer and electron microprobe data is $Alm_{90}Grs_{2.7}Py_{2.3}Ski_{4.5}$ (Woodland et al. 1995) and we refer to it as 'Alm90' in this paper.

The spessartine is a Smithsonian sample, NMNH-47705, from Amelia Courthouse, Amelia Co., VA, USA. A new Mössbauer analysis shows that the Fe^{3+} proportion is quite low, about 3% of total Fe, indicating that there is no significant skiagite component, less than 0.01 molar. With this constraint new microprobe analyses gave a composition $Sps_{81}Alm_{15}Grs_3And_1$ (Table S1). We refer to it as 'Sps81'.

X-ray diffraction

Garnets containing Fe and Mn are liable to oxidise at high temperatures in air, so a small portion of each of Alm90 and Sps81 garnets was ground to a fine powder and each was sealed in a glass capillary with iron wire under argon to prevent oxidation. Quartz was added as an internal standard for temperature. Powder diffraction data were collected from both samples with nominally identical procedures on the same days on the beamline X04SA (Willmott et al. 2013) of the Swiss Light Source at the Paul Scherrer Institute, Switzerland with a 'MYTHEN III' linear detector with intrinsic resolution of 3.7 mdeg. in 2θ, covering 120 deg. in 2θ (Andrä et al. 2024). In our experiments the data were collected up to $2\theta = 70°$ with an X-ray wavelength of 0.70893 Å calibrated from the NIST SRM-640c Si standard at room temperature.

Two data collection runs were performed for each sample. The first one used a Cryostream cooler, with nominal (gas jet) temperatures starting at 90 K and going up to 480 K, and the second run used a hot air blower, with nominal gas jet temperatures starting at room temperature and going up to 873 K before cooling in steps to room temperature. Each data collection was performed at a constant sample temperature. Patterns were fitted by automated sequential Rietveld refinement with Topas v.6 (Coelho 2018), keeping the profile function fixed after refinement at room temperature. Because of the similar X-ray scattering power of Mn and Fe, refinements were performed with fixed site occupancies corresponding to the end-member compositions but the variable coordinates and isotropic displacement factors in both garnet and quartz were refined, as well as Gaussian size broadening and Lorentzian strain broadening. In the Alm90 sample the peaks coming from spessartine contamination were fitted in the refinement with a model for spessartine. Further details are provided in the supplementary information.

Using an internal standard with symmetry lower than cubic allows the internal consistency of the two datasets to be evaluated, independent of the uncertainties from temperature calibrations, in two ways; by plotting the unit-cell

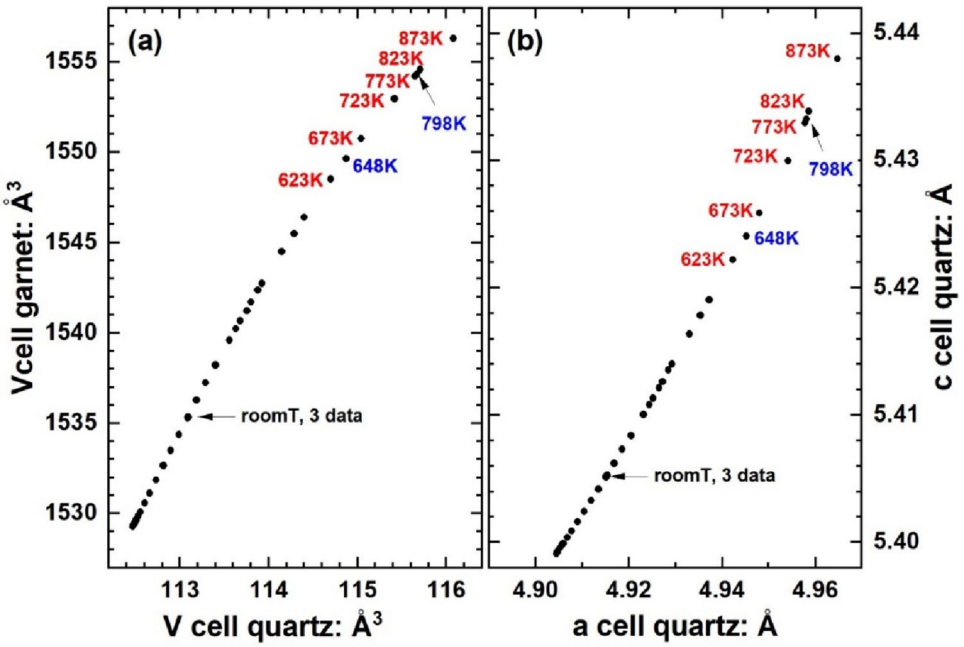

Fig. 1 The internal consistency of the cell parameters obtained by Rietveld refinement are illustrated by plotting (a) the unit-cell volumes of garnet against quartz and (b) the *a*- and *c*-cell parameters of quartz. Numbers indicate the nominal jet temperatures of the hot air blower. Some of the data collected on cooling are indicated by blue numbers and they fall on the trends of data collected on heating (red numbers), indicating no hysteresis between the heating and cooling cycle. There is no discontinuity in slope between the data collected with the Cryostream and the hot air blower. The data shown are for the Alm90 sample, plots of the Sps81 data are very similar (Figure S1)

volume of garnet against that of quartz (Fig. 1a) and by plotting the *a*- and *c*-cell parameters of quartz against one another (Fig. 1b). The smooth trends in both plots indicate that there are no outliers in the dataset and that the data collected on cooling agree within uncertainties with the trends of data collected during the heating cycle. Together with no significant difference in the cell parameters collected at nominal room temperature before and after heating this confirms the stability of the diffractometer over the period of the experiment, and that the garnets did not undergo any irreversible oxidation or other chemical change.

Above room temperature the 'full curved boundary' EoS of quartz (Angel et al. 2017a) was used to determine the temperatures from the measured unit-cell volumes of the quartz in each sample. The Cryostream jet temperatures were used for the data collected below room temperature. Complete details of the temperature calibrations and estimation of the temperature uncertainties are provided in the supplementary information along with the refined unit cell parameters in Tables S2 and S3. Note that the actual maximum sample temperatures reached in the two measurements differ by 12 K at the same highest nominal gas jet temperature, which probably results from small differences in the gas flow rate below the precision of the flowmeter. This reinforces the need to use internal standards as we did to determine temperatures in high-T experiments with gas blowers.

Brillouin scattering

For both almandine and spessartine samples a randomly oriented platelet was cut, ground to a final thickness of approximately 200 μm using SiC grinding paper and polished with diamond to a final 1 μm diamond particle size. The two faces of each platelet were parallel within 0.2 degrees. Acoustic velocities were determined by Brillouin scattering measurements performed in symmetric forward scattering geometry (Grimsditch and Polian 1989; Speziale et al. 2014). The 532.15 nm line of a Nd-doped YVO_4 laser source was focused on the sample. The scattered light was collected at an external scattering angle of 60 ± 0.1 degree. The scattered light was analysed by a tandem Fabry-Perot spectrometer (Sandercock 1982) and detected by a solid-state single photon count detector. A total of 76 spectra were collected in 41 directions for almandine and 57 spectra in 35 directions for spessartine. The individual spectra featured two acoustic phonon modes (one quasi-longitudinal mode and one quasi-transverse mode). The second quasi-transverse acoustic mode was never observed due to the very low elastic anisotropy of the two garnets, which causes spectral overlap of the two quasi-transverse modes and unfavourable acousto-optic coupling causing weak intensity of one of the two quasi-transverse modes which cannot be alleviated in the geometry used for these measurements (Cummins and Schoen 1972). In 9 spectra for almandine and 1 spectrum for spessartine the signal of the quasi-longitudinal phonon mode was extremely weak, and it was not processed.

In order to obtain the elastic moduli from the Brillouin scattering data the true density of the samples is needed. This requires the true volume at 298 K. For this purpose alone we scaled the measured unit cell volumes (Tables S2,3) to a molar volume for quartz of 22.69 cm^3/mol (Holland and Powell 2011), which corresponds to a unit-cell volume of 113.036 $Å^3$. This scaling introduces a correction

Table 1 Elastic tensors of samples Alm90 and Sps81 at room conditions

	Units	Alm90	Sps81
Composition	mol%	Alm90 Grs2.7 Py2.3 Ski4.5	Sps81 Alm15 Grs3 And1
Molar volume	cm^3mol^{-1}	115.51	117.91
Density	$g.cm^{-3}$	4.302	4.192
c_{11}	GPa	302.0(5)	303.1(4)
c_{12}	GPa	111.3(4)	109.5(4)
c_{44}	GPa	93.3(1)	93.6(2)
K_S	GPa	174.9(4)	174.0(4)
G_S [1]	GPa	94.1(2)	94.9(2)

Note [1] the Reuss and Voigt average adiabatic shear moduli are the same within the estimated uncertainties

to our measured volumes of approximately 0.03% to give the volumes and densities in Table 1. The three independent components of the elastic tensor of each garnet (Table 1) were determined using these densities by least squares fitting of a set of Christoffel's equations to the measured acoustic velocities, refining both the values of the tensor components and the orientation of the plate simultaneously. Uncertainties in the density values are difficult to estimate, but a change in the spessartine content by 1 mol% (and almandine by an opposite amount) changes the calculated density by only 0.0002, so the uncertainties in the reported moduli are dominated by the uncertainties from the fitting of the velocities.

Equations of state

Our guiding principle in determining the EoS of almandine and spessartine was to use the largest possible number of consistent data for the pressure, temperature and PT variation of the bulk modulus and volume of each of these garnets. We therefore used the methods described in detail in Angel et al. (2022). In brief, to avoid differences introduced by instrument calibrations and minor variations in composition all sets of volume measurements were scaled to the value measured in the same study at room conditions, and then these were scaled to the standard molar volume (Holland and Powell 2011) of the garnet. In doing so, we have implicitly assumed that the elastic properties of the end-member compositions are experimentally indistinguishable from those of our measured samples; this seems justified by the results, as we discuss later.

Datasets without measurements at room conditions were used with refined scale factors (Ehlers et al. 2022), as were elasticity data derived from experiments on polycrystalline samples to account for systematic effects such as preferred orientation and buffer-rod corrections. Data consistency between studies of the same type was assessed by direct comparison of the data values and not by comparison of parameters of equations fitted to the data. After initial assessment and elimination of outlier data, least-squares refinement of EoS parameters was performed to all of the available volume and bulk moduli simultaneously with the EosFit-7c program (Angel et al. 2014a; Milani et al. 2017). Data were evaluated for agreement with the refined parameters, with aberrant data being excluded from subsequent refinements. More details about data sources and our detailed evaluation of them are provided in Tables S4 and S5.

Table 2 Parameters for *q*-compromise MGD plus BM3 EoS

	Almandine	Spessartine	Pyrope*	Grossular*
V_0 : cm^3/mol	115.25	117.92	113.13	125.35
K_{0T} : GPa	174.1(4)	172.2(7)	169.3(3)	167.0(2)
K_0'	5.56(14)	5.6(3)	4.55(5)	5.07(8)
θ_D : K	549(4)	569(5)	771(28)	750(13)
γ_0	1.186(4)	1.135(6)	1.185(12)	1.156(6)
K_{0S} : GPa	175.6(4)	173.5(7)	170.7(4)	168.2(3)

*Parameters from Angel et al. (2022)

As for grossular and pyrope (Angel et al. 2022), we found that *q*-compromise Mie-Grüneisen-Debye thermal pressure EoS (Angel et al. 2020) with third-order Birch-Murnaghan EoS (e.g. Anderson 1995) for the compression at room temperature adequately describe the data for almandine and spessartine with the minimum number of refinable parameters. The final refined EoS parameters are provided in Table 2 along with those for pyrope and grossular (Angel et al. 2022) for comparison. They are also available in the supplementary information for this paper, and at www.rossangel.com and as .eos files for the EosFit software suite. A full comparison of the properties of the new EoS for almandine and spessartine with those of the previous EoS (Angel et al. 2022) is provided in Figures S2-S9.

Almandine

The thermal expansion of our previous EoS (Angel et al. 2022) was based solely on the data of Skinner (1956) for a synthetic almandine of end-member composition, with an adjustment to the reported temperatures derived from a comparison of his results for pyrope and grossular to more modern data. More recent data from Galkin and Gartvich (2015) that was not considered in Angel et al. (2022) seem to support this rescaling, but they do not agree with either the 100 K datum of Armbruster et al. (1992) or our new data (Fig. 2). The almandine volume at 106 K from Galkin and Gartvich (2015) corresponds to the value we measured at 200 K, suggesting that their temperature calibration was in error. Their paper appears to suggest that they used an internal Si standard for calibration of the 2θ data, but there

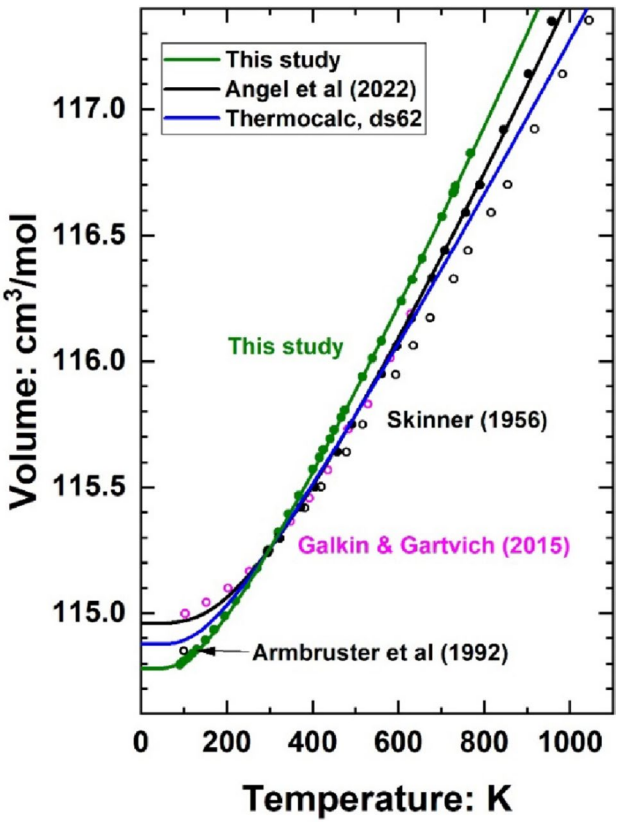

Fig. 2 Thermal expansion data for almandine. Data point colours correspond to the coloured labels. In the analysis of Angel et al. (2022) the original data of Skinner (1956) for Alm100, shown here as open symbols, were shifted down in temperature to the values shown as solid symbols on the basis of his results for pyrope and grossular and used in the refinement of the EoS. The data collected in this study exhibit a much higher thermal expansion coefficient and agree with the datum of Armbruster et al. (1992) at 100 K

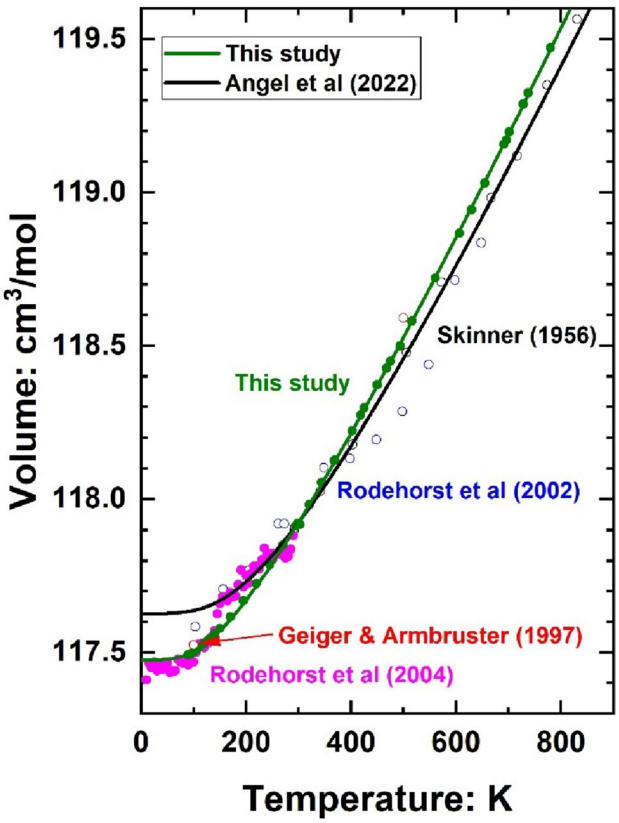

Fig. 3 Thermal expansion of spessartine showing the data available for the analysis of Angel et al. (2022) and the EoS derived in that study (black line), overlain with data for the Sps81 sample. The Sps81 data suggest that the data of Rodehorst et al. (2004) below 140 K are probably correct instead of that above 140 K

is no indication of the measured cell parameter values for Si at non-ambient temperatures, and it may be that their temperature values relied on previous calibrations. Without this information, the data of Galkin and Gartvich (2015) cannot be evaluated or used.

Our new data agree with the 100 K single-crystal datum of Armbruster et al. (1992) and clearly show that the Debye temperature of almandine is much lower than the MGD EoS published in Angel et al. (2022). To determine a new EoS we used these 34 VT data and the K_{0S} = 174.9(4) GPa for sample Alm90 from the current study together with 20 room-temperature PV data (Zhang et al. 1999; Milani et al. 2015) and 49 P-T-Ks data (Arimoto et al. 2015). Details of these datasets and the reasons for excluding other published datasets for inconsistency are given in Table S4.

Final parameters for the EoS fitted to all of these data are listed in Table 2. The previous analysis (Angel et al. 2022) showed that the K_S data above 1100 K from Arimoto et al. (2015) were not consistent with the previous rescaled measurements of the thermal expansion (Skinner 1956). In contrast, we now find that the entire dataset of Arimoto et al. (2015), without their room PT value, is consistent with the new VT data fitted with a *q*-compromise MGD EoS (Fig. 2), with very little change in the parameter values when the highest-T data are included. The PV behaviour at ambient temperature of the new EoS is indistinguishable from that of Angel et al. (2022) but the higher thermal expansion results in significantly steeper isochors which lie at ca. 0.3 GPa higher pressures at 700 °C (Figure S4).

Spessartine

Above room temperature our data for Sps81 (Fig. 3) agree with the single-crystal datum of Geiger and Armbruster (1997) at 500 K and indicate significantly larger thermal expansion than the EoS of Angel et al. (2022) based on the data of Skinner (1956), consistent with his results for pyrope, grossular and almandine.

The only previously available low-temperature data for spessartine (Rodehorst et al. 2004) has a step in the volume at ~145 K, which does not correspond to any phase

transition. In their previous analysis Angel et al. (2022) decided that the lower-T data were in error, and that the data from 150 K to room temperature were correct. Our new data for Sps81 now indicate that this conclusion was wrong, and that the lower T data of Rodehorst et al. (2004) are approximately correct, at least in the range 140–100 K (Fig. 3). The deviation of the Rodehorst et al. (2004) data below 100 K from an extrapolation of the Sps81 data using the *q*-compromise MGD EoS may reflect the over-simplification of the phonon density of states in the MGD EoS, so we did not use the data of Rodehorst et al. (2004). The parameters of the MGD EoS of spessartine was therefore determined from the 38 VT data and K_{0S} = 174.0(4) GPa for sample Sps81 from the current study, plus 8 PV data (Zhang et al. 1999) and 23 PVT data (Gréaux and Yamada 2014) for synthetic Sps100 refining the data scale factors for both of these datasets from the literature. Full details are provided in Table S5, and final parameters for the EoS fitted to all of these data are listed in Table 2. Note that the value of K_{0S} = 173.5(7) GPa is within 1 esu of the value we determined by Brillouin scattering. If a value of K_{0S} = 178.8(8) GPa for Sps95Alm5 (Bass 1989) is used instead in the fit of the EoS parameters, the refined value of K_{0S} is more than 2 esu's lower than the experimental value suggesting that it is less consistent with the volume data (Zhang et al. 1999; Gréaux and Yamada 2014) for end-member spessartine.

The PV behaviour at room temperature of the new EoS for spessartine is indistinguishable from that published by Angel et al. (2022) because the lower value of K_{0T} is compensated by an increase in K'_0 from 4.6(3) to 5.6(3), the same value as for almandine. In combination with the increase in thermal expansion coefficient, the decrease in bulk modulus means that the isochors of the new EoS of spessartine are indistinguishable (Figure S8) from those of the EoS of Angel et al. (2022).

Almandine-spessartine solid solution

The difference in adiabatic bulk moduli between almandine and spessartine end-member compositions from our EoS is only 2.1(8) GPa (Table 2), so there is no distinguishable difference between the Reuss and Voigt bounds of the bulk moduli predicted for intermediate compositions (Fig. 4). For almandine-rich compositions the available experimental measurements are in mutual agreement, and our value of K_{0S} determined by Brillouin scattering for the Sps81 sample also agrees with the Reuss and Voigt bounds, as does the datum for the intermediate composition of Verma (1960).

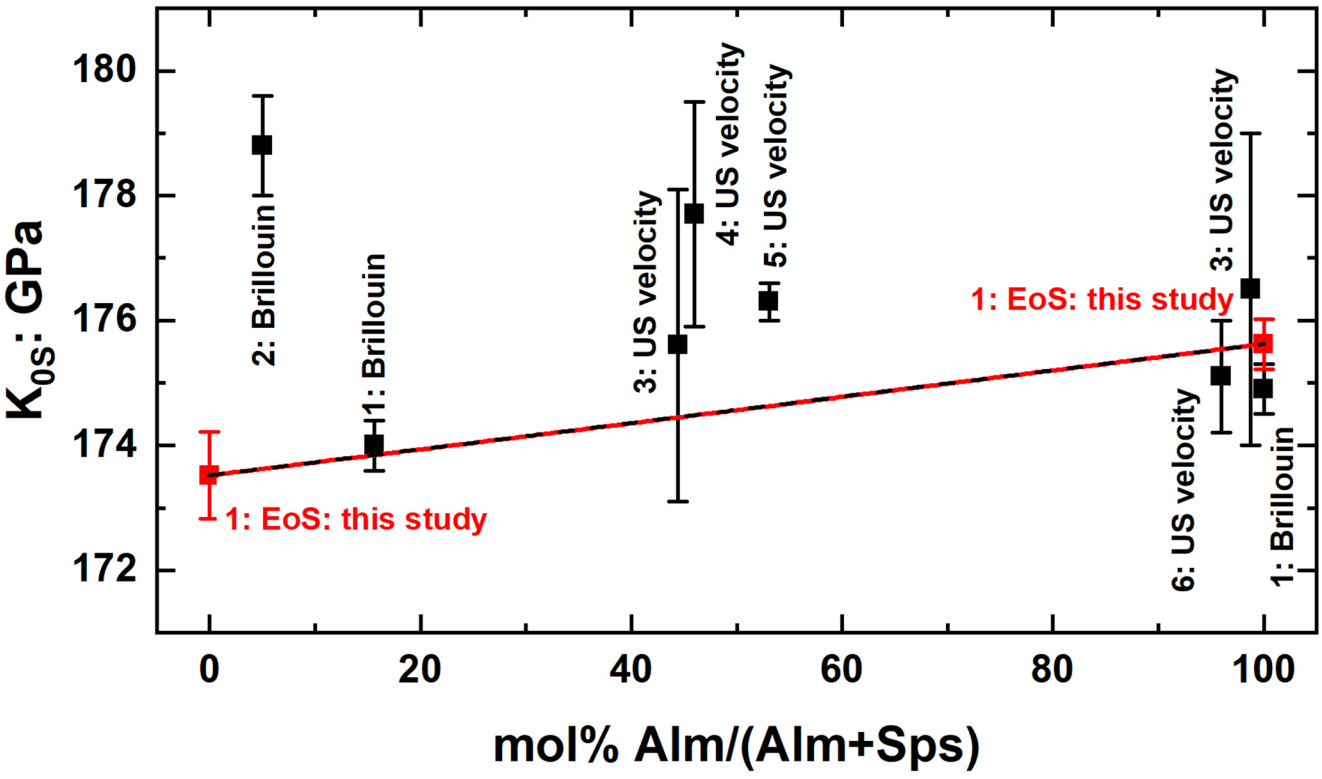

Fig. 4 The variation of adiabatic bulk modulus at room conditions across the spessartine-almandine join. Data are plotted as the molar ratio of almandine to spessartine ignoring other components. Because the difference between the end-member moduli in our EoS is ca. 1.2% there is no significant difference between the Reuss (red solid line) and Voigt (black dashed line) bulk moduli predicted for intermediate compositions. Sources of the data are: 1 - this study, 2 - Bass (1989), 3 - Verma (1960), 4 - Wang andSimmons (1974), 5 - Isaak and Graham (1976), 6 - Wang and Ji (2001)

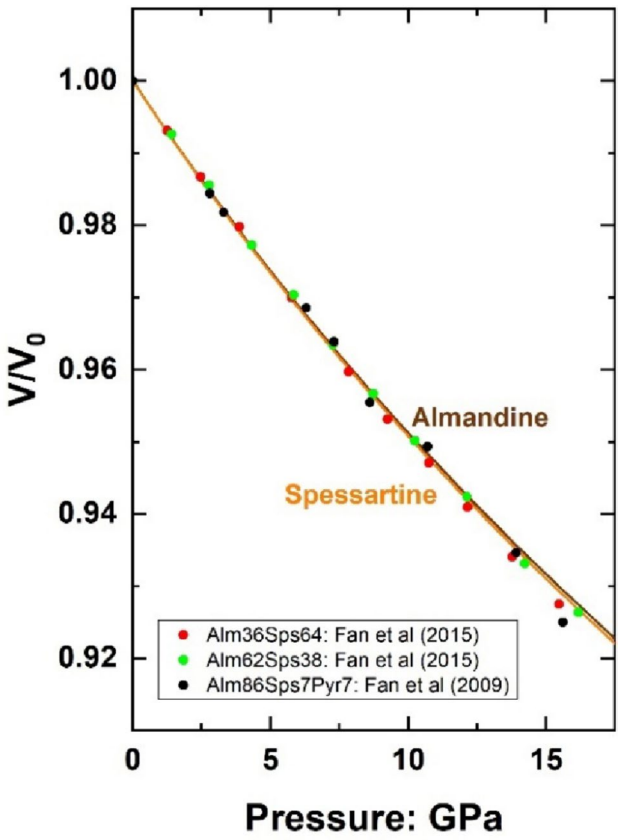

Fig. 5 Compressional data (Fan et al. 2009, 2015) for intermediate spessartine-almandine garnets show data scatter both above and below the EoS for the endmembers (lines). Therefore, there is no experimental evidence for the intermediate compositions having EoS that deviate beyond the Reuss and Voigt bounds derived from the endmembers. The data of Fan et al. (2009) also indicate that there is no significant effect on the EoS of 7 mol% pyrope component

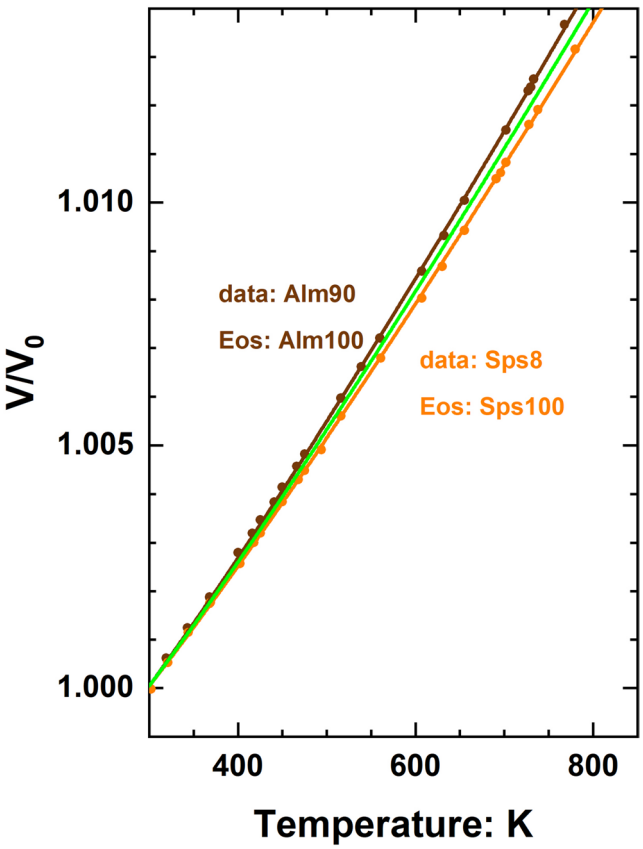

Fig. 6 A comparison of the thermal expansion of almandine and spessartine garnets. The green line represents the volumes of an Alm-50Sps50 composition calculated by Eq. (1) from the EoS of the two endmembers

$$\frac{V\,(P,T)}{V_0} = \frac{X_{alm}V_{alm}\,(P,T) + X_{sps}V_{sps}\,(P,T)}{X_{alm}V_{alm}\,(1atm,298K) + X_{sps}V_{sps}\,(1atm,298K)} \quad (1)$$

The compressional part of the EoS of spessartine and almandine expressed as fractional compression, V/V_0, are also indistinguishable (Fig. 5) and there is no evidence from compressional studies of intermediate compositions (Fan et al. 2009, 2015) of any excess in their elastic properties or deviations beyond the Reuss and Voigt bounds derived from the end members. The remaining scatter of K_{0S} values about the ideal mixing line (Fig. 5) may be due to experimental uncertainties and the effects of other compositional components in the measured samples.

We have been unable to locate any published data for the thermal expansion of intermediate composition almandine-spessartine garnets, although the EoS and data (Fig. 6) suggest that differences in V/V_0 could be measured experimentally to determine how the weak non-ideality of the volume of mixing at room conditions (e.g. Geiger 2016) evolves with temperature. In the absence of such data, we suggest that the V/V_0 of these garnets at any P and T can be approximated by an ideal mixing model of the end members, in which X_{alm} and X_{sps} are the molar fractions of the two components, and the volumes V_{alm} and V_{sps} on the right-hand side are calculated from the EoS of the corresponding end members. This calculation can be performed in the mphase utility of the EosFit7c program (Angel et al. 2023) and are shown for the 50:50 composition in Fig. 6. If a value for the actual volume is required, then we recommend that the value from Eq. (1) is multiplied by the V_0 from an appropriate model for the excess volume of mixing at room conditions.

Implications for piezobarometry

We have shown that almandine-spessartine garnets have indistinguishable P-V behaviour at room temperature (Fig. 5) very similar to the previous EoS (e.g. Angel et al. 2022). Therefore the P_{foot}, the pressure of the entrapment isomeke at room temperature (Angel et al. 2014b),

calculated from a measured inclusion pressure (P_{inc}) in an almandine-spessartine garnet host does not change significantly with the new EoS, and neither is it sensitive to the composition of the garnet host; if P_{inc} = 1.0 GPa for a quartz inclusion, then the P_{foot} for almandine and spessartine hosts differ by 0.002 GPa. The implications of the new EoS for host-inclusion piezobarometry therefore depend on the slopes of the entrapment isomekes, which are determined by the ratio of the difference in thermal expansion coefficients of host and inclusion to the difference in their respective compressibilities (e.g. Angel et al. 2014b; Kohn et al. 2023).

Quartz has a high thermal expansion coefficient below the α-β phase boundary and therefore the increase of the thermal expansion coefficients of the garnets only slightly reduces the slopes of the isomekes for quartz in garnet (QuiG). The new almandine EoS gives isomekes with α-quartz that lie about 0.1 GPa lower at 2 GPa and 800 °C than the published EoS (Fig. 7a). For spessartine the compensating effects of slightly lower bulk modulus (and higher compressibility) at low pressures and higher thermal expansion coefficient lead to QuiG isomekes that are < 0.03 GPa lower than previously (Fig. 7b). Given the typical uncertainties in P_{trap} of 0.1–0.2 GPa (e.g. Gilio et al. 2021; Gilio et al. 2025) arising from uncertainties in the measurement of P_{inc}, these differences are not significant. In addition, the isomekes for almandine and spessartine (Fig. 7c) for the same P_{inc} are separated by less than 0.1 GPa throughout the stability field of α-quartz, so 0.1 GPa is the maximum uncertainty for P_{trap} even if the almandine: spessartine ratio of the garnet host is unknown. If the composition is known, the linear addition in proportion to their molar proportions of P_{trap} values calculated with the end-members (Eq. 7 of Angel et al. 2022) instead of via Eq. (1) leads to insignificant errors in P_{trap} at the 0.002 GPa level.

The β-phase of quartz has a very small or zero volume thermal expansion coefficient (e.g. Carpenter et al. 1998; Angel et al. 2017a), so the resulting large contrast to the thermal expansion coefficients of the garnets means that the slopes of their isomekes with β-quartz are not significantly changed by the new EoS. However, for both garnets the slightly lower isomeke pressures with α-quartz have the effect of significantly reducing the P and T at which a given isomeke crosses the α-β-phase boundary. This shifts the isomekes to lower temperatures in the stability field of β-quartz. by ca. 70 °C (almandine) and ca. 45 °C (spessartine) (Figs. 7a, b).

Isomekes of zircon with garnet (ZinG) are steeper in P-T space (Fig. 8) than those of QuiG because the compressibility of zircon is more similar to that of garnet than is quartz. This makes ZinG a good geothermometer. As a consequence, the slopes of the isomekes are more sensitive to

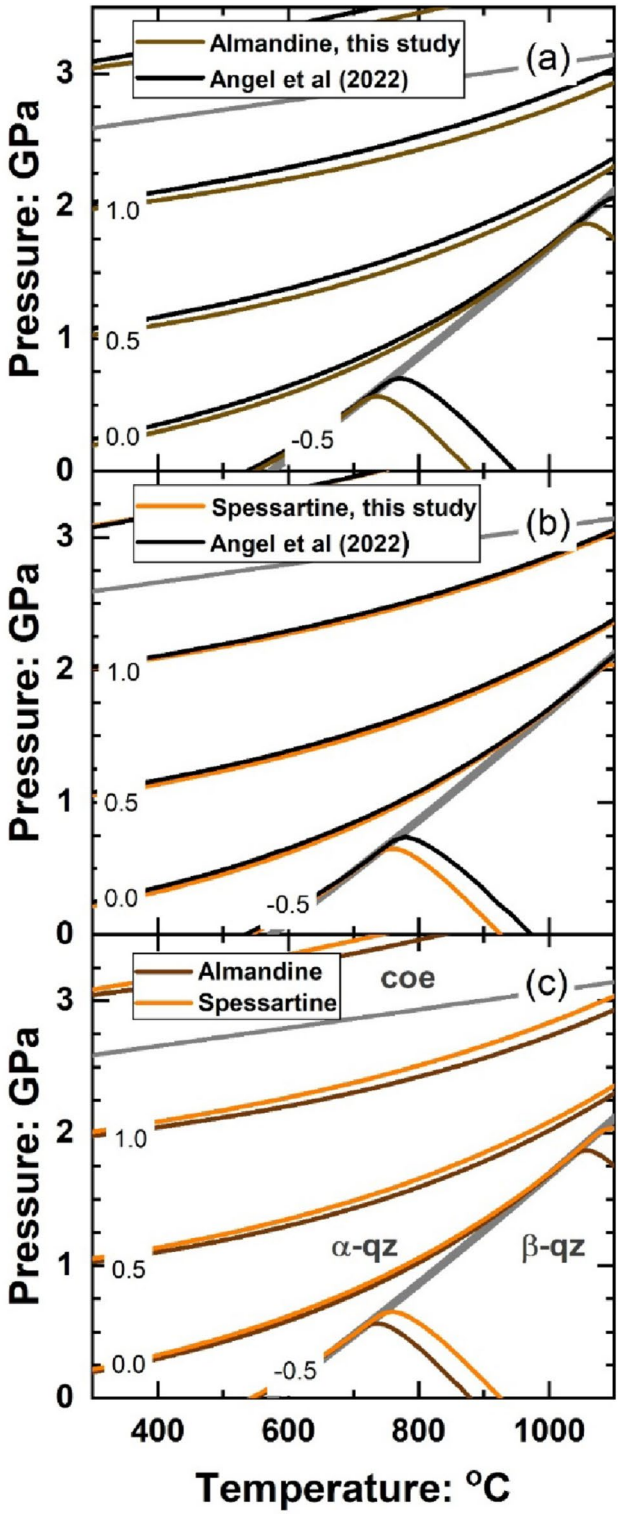

Fig. 7 Entrapment isomekes with quartz (Angel et al. 2017a) of the new *q*-compromise MGD EoS of (**a**) almandine and (**b**) spessartine compared to those of the EoS of Angel et al. (2022). **c** Comparison of QuiG isomekes for almandine and spessartine with the new EoS. Numbers in boxes are the inclusion pressures in GPa that would be measured at room conditions for inclusions trapped on the isomekes. The two grey lines are the phase boundaries for α-quartz = coesite (Bose and Ganguly 1995) and α– = β–quartz. Stability fields are labelled in part (**c**)

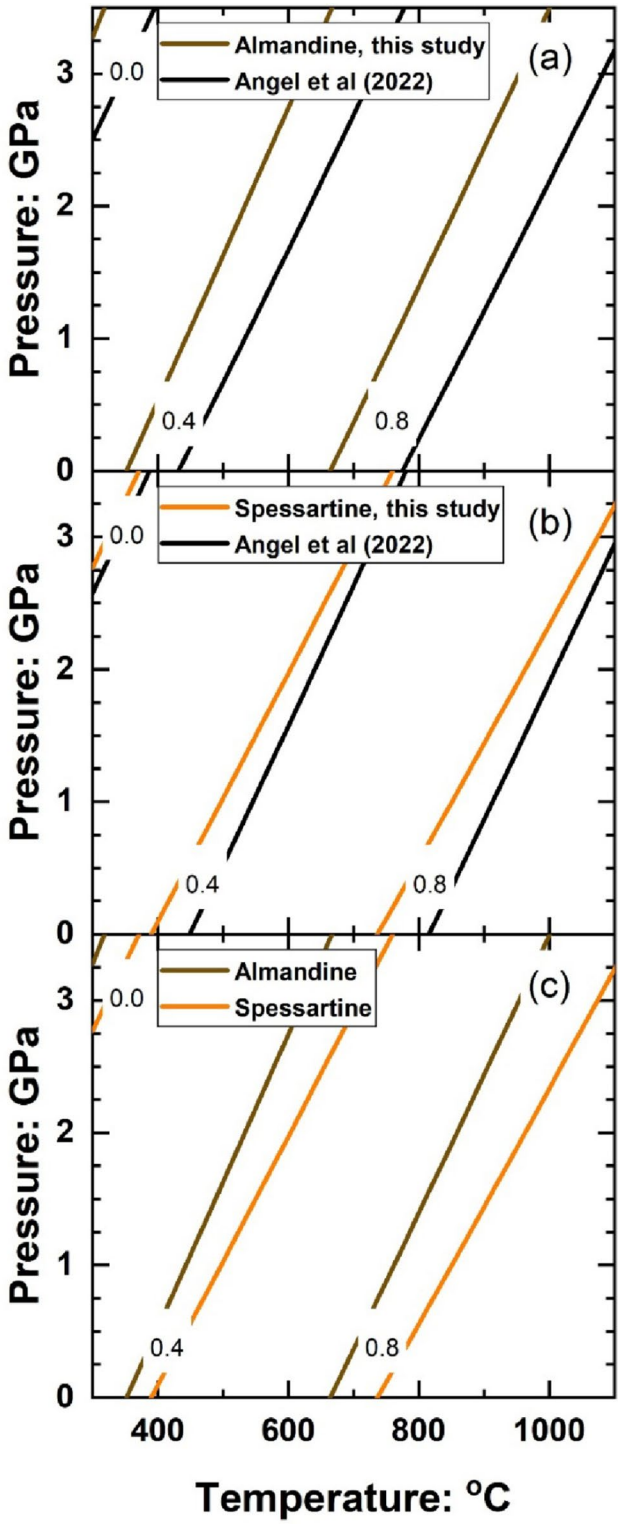

Fig. 8 Entrapment isomekes with zircon (Ehlers et al. 2022) of the new *q*-compromise MGD EoS of (a) almandine and (b) spessartine compared to those of the EoS of Angel et al. (2022). (c) Comparison of ZinG isomekes for almandine and spessartine with the new EoS. Numbers in boxes are the inclusion pressures in GPa that would be measured at room conditions for inclusions trapped on the isomekes

the contrast in thermal expansion coefficients of host garnet and zircon inclusions. Both new EoS result in significantly steeper isomekes that lie ca. 100 °C (almandine) and ca. 50 °C (spessartine) below those of the previous EoS at geologically relevant temperatures (Fig. 8a, b).

For ZinG, and QuiG in the stability field of β-quartz, the steeper isomekes mean that entrapment conditions are better expressed as temperatures at a given pressure. In these two cases, the isomekes for almandine and spessartine are far enough apart in temperature (Figs. 7c and 8c) that the effect of the almandine:spessartine ratio on the entrapment isomekes should be considered. This can be done by using the volumes of the garnet calculated via Eq. 1. Or entrapment temperatures can be reliably estimated within 5 °C by a linear combination of the T_{trap} calculated for the two end-members in a manner similar to Eq. 7 of Angel et al. (2022), thus:

$$T_{trap}^{mix} = X_{alm}T_{trap}^{alm} + X_{sps}T_{trap}^{sps} \quad (2)$$

Supplementary Information The online version contains supplementary material available at https://doi.org/10.1007/s00410-025-02294-6.

Acknowledgements The Sps81 sample was kindly provided by Jeff Post and Paul Powhat of the National Museum of Natural History at the Smithsonian Institution. Beamtime at the X04SA beamline of the Swiss Light Source was kindly provided by the Paul Scherrer Institut. Support for the travel to the SLS was provided by the European Union's Horizon 2020 research and innovation program grant agreement 714936 TRUE DEPTHS to Matteo Alvaro. This work benefited from discussions and suggestions from Mattia Gilio (Pavia) and Nicola Campomenosi (Genova), and the comments of Frank Spear (RPI) and an anonymous reviewer. We thank Megan Koch and Jay Thomas (Syracuse) and Joe Gonzalez (New York State Museum) for sharing their experimental data on almandine-hosted inclusions prior to publication and for testing the EoS.

Author contributions Project conception and design: Hovis, Angel, Alvaro, Tribaudino. Data collection: Angel, Morana, Casati, Speziale, Woodland. Data analysis: Angel, Morana, Casati, Speziale, Woodland, Tribaudino. Manuscript drafting and review: all authors.

References

Anderson OL (1995) Equations of state of solids for geophysics and ceramic science. Oxford University Press, Oxford, UK

Andrä M, Bergamaschi A, Baruffaldi F, Brückner M, Carulla M, Casati N, Cervellino A, Dinapoli R, Fröjdh E, Greiffenberg D, Hasanaj S, Heymes J, Hinger V, Kozlowski P, Cuenca CL, Meister D, Mezza D, Moustakas K, Mozzanica A, Paton K, Christian Ruder C, Scagnoli V, Smolentsev G, Schmitt B, Thattil D, Xiea X, Zhang J (2024) MYTHEN III: advancements in single photon counting detectors for synchrotron powder diffraction experiments. J Synchrotron Radiat 32:365–377. https://doi.org/10.1107/S1600577525000438

Angel RJ, Gonzalez-Platas J, Alvaro M (2014a) EosFit7c and a fortran module (library) for equation of state calculations. Z für Kristallographie 229:405–419

Angel RJ, Mazzucchelli ML, Alvaro M, Nimis P, Nestola F (2014b) Geobarometry from host-inclusion systems: the role of elastic relaxation. Am Mineral 99:2146–2149

Angel RJ, Alvaro M, Miletich R, Nestola F (2017a) A simple and generalised P-T-V EoS for continuous phase transitions, implemented in EosFit and applied to quartz. Contrib Miner Petrol 172:29. https://doi.org/10.1007/s00410-017-1349-x

Angel RJ, Mazzucchelli ML, Alvaro M, Nestola F (2017b) EosFit-Pinc: A simple GUI for host-inclusion elastic thermobarometry. Am Mineral 102:1957–1960. https://doi.org/10.2138/am-2017-6190

Angel RJ, Alvaro M, Schmid-Beurmann P, Kroll H (2020) Commentary on 'Constraints on the equations of state of stiff anisotropic minerals: rutile, and the implications for rutile elastic barometry'. Mineral Mag 84:339–347. https://doi.org/10.1180/mgm.2020.14

Angel RJ, Gilio M, Mazzucchelli ML, Alvaro M (2022) Garnet eos: a critical review and synthesis. Contrib Miner Petrol 177:54. https://doi.org/10.1007/s00410-022-01918-5

Angel RJ, Mazzucchelli ML, Musiyachenko KA, Nestola F, Alvaro M (2023) Elasticity of mixtures and implications for piezobarometry of mixed-phase inclusions. Eur J Mineral 35:461–468. https://doi.org/10.5194/ejm-35-461-2023

Arimoto T, Gréaux S, Irifune T, Zhou C, Higo Y (2015) Sound velocities of $Fe_3Al_2Si_3O_{12}$ Almandine up to 19 GPa and 1700 K. Phys Earth Planet Inter 246:1–8. https://doi.org/10.1016/j.pepi.2015.06.004

Armbruster T, Geiger CA, Lager GA (1992) Single-crystal X-ray structure study of synthetic Pyrope Almandine garnets at 100 and 293 K. Am Mineral 77:512–521

Bass JD (1989) Elasticity of grossular and spessartite garnets by Brillouin spectrsocopy. J Phys Res 94:7621–7628

Bose K, Ganguly J (1995) Quartz-coesite transition revisited: reversed experimental determination at 500-1200°C and retrieved thermochemical properties. Am Mineral 80:231–238

Campomenosi N, Angel RJ, Alvaro M, Mihailova B (2023) Resetting of Zircon inclusions in garnet: implications for elastic thermobarometry. Geology 51:23–27. https://doi.org/10.1130/G50431.1

Carpenter MA, Salje EKH, Graeme-Barber A, Wruck B, Dove MT, Knight KS (1998) Calibration of excess thermodynamic properties and elastic constant variations associated with the alpha-beta phase transition in quartz. Am Mineral 83:2–22

Coelho AA (2018) TOPAS and TOPAS-Academic: an optimization program integrating computer algebra and crystallographic objects written in C++. J Appl Crystallogr 51:210–218

Cummins HZ, Schoen PE (1972) Linear scattering from thermal fluctuations. In: Arecchi FT, Schultz-Dubois EO (eds) Laser handbook. North Holland, Amsterdam, pp 1029–1076

Ehlers AM, Zaffiro G, Angel RJ, Boffa-Ballaran T, Carpenter MA, Alvaro M, Ross NL (2022) Thermoelastic properties of zircon: implications for geothermobarometry. Am Mineral 107:74–81. https://doi.org/10.2138/am-2021-7731

Fan DW, Zhou WG, Liu CQ, Liu YG, Wan F, Xing YS, Liu J, Bai LG, Xie HS (2009) The thermal equation of state of $(Fe_{0.86}Mg_{0.07}Mn_{0.07})_3Al_2Si_3O_{12}$ Almandine. Mineral Mag 73:95–102. https://doi.org/10.1180/minmag.2009.073.1.95

Fan D, Xu J, Ma M, Liu J, Xie H (2015) P–V–T equation of state of spessartine–almandine solid solution measured using a diamond anvil cell and in situ synchrotron X–ray diffraction. Phys Chem Miner 42. https://doi.org/10.1007/s00269-014-0700-2

Galkin V, Gartvich Y (2015) Thermal expansion and evaluation of Almandine heat capacity. J Therm Anal Calorim 122:1239–1244. https://doi.org/10.1007/s10973-015-4768-9

Geiger CA (2016) A Tale of two garnets: the role of solid solution in the development toward a modern mineralogy. Am Mineral 101:1735–1749. https://doi.org/10.2138/am-2016-5522

Geiger CA, Armbruster T (1997) $Mn_3Al_2Si_3O_{12}$ spessartine and $Ca_3Al_2Si_3O_{12}$ grossular garnet: structural dynamic and thermodynamic properties. Am Mineral 82:740–747

Gilio M, Angel RJ, Alvaro M (2021) Elastic geobarometry: how to work with residual inclusion strains and pressures. Am Mineral 106:1530–1533. https://doi.org/10.2138/am-2021-7928

Gilio M, Angel RJ, Mazzucchelli ML, Alvaro M (2025) The pressure-induced stiffening of quartz and its effect on the strain-stress relationship. Implications for elastic geobarometry. Lithos. https://doi.org/10.1016/j.lithos.2025.108210. 514–515:108210 doi

Gréaux S, Yamada A (2014) P–V–T equation of state of $Mn_3Al_2Si_3O_{12}$ spessartine Garnet. Phys Chem Miner 41:141–149. https://doi.org/10.1007/s00269-013-0632-2

Grimsditch M, Polian A Brillouin scattering at high pressures. In: Polian A, Loubeyre P, Boccara N (eds) NATO advanced research workshop / European physical society workshop on simple molecular systems at very high Density, les Houches, France, 1989. NATO ASI series. Series B,. Plenum, New York

Holland TJB, Powell R (2011) An improved and extended internally consistent thermodynamic dataset for phases of petrological interest, involving a new equation of state for solids. J Metamorph Geol 29:333–383. https://doi.org/10.1111/j.1525-1314.2010.00923.x

Isaak D, Graham E (1976) The elastic properties of an almandine-spessartine Garnet and elasticity in the Garnet solid solution series. J Phys Res 81:2483–2489

Kohn MJ, Mazzucchelli ML, Alvaro M (2023) Elastic thermobarometry. Annu Rev Earth Planet Sci 51. https://doi.org/10.1146/annurev-earth-031621-112720

Milani S, Nestola F, Alvaro M, Pasqual D, Mazzucchelli ML, Domeneghetti MC, Geiger C (2015) Diamond–garnet geobarometry: the role of Garnet compressibility and expansivity. Lithos 227:140–147

Milani S, Angel RJ, Scandolo L, Mazzucchelli ML, Boffa-Ballaran T, Klemme S, Domeneghetti MC, Miletich R, Scheidl KS, Derzsi M, Tokar K, Prencipe M, Alvaro M, Nestola F (2017) Thermoelastic behaviour of grossular garnets at high pressures and temperatures. Am Mineral 102:851–859. https://doi.org/10.2138/am-2017-5855

Rodehorst U, Carpenter MA, Boffa-Ballaran T, Geiger CA (2004) Local structural heterogeneity, mixing behaviour and saturation effects in the grossular–spessartine solid solution. Phys Chem Miner 31:387–404. https://doi.org/10.1007/s00269-004-0410-2

Sandercock JR (1982) Trends in Brillouin scattering: studies of opaque materials, supported films, and central modes. In: Cardona M, Güntherodt G (eds) Light scattering in solids III. Topics in applied physics, vol 51. Springer, Berlin, Heidelberg, pp 173–206. doi:https://doi.org/10.1007/3540115137_6

Skinner BJ (1956) Physical properties of end.members of the Garnet group. Am Mineral 41:428–436

Speziale S, Marquardt H, Duffy T (2014) Brillouin scattering and its application in geosciences. Rev Mineral Geochem 78:543–603

Verma RK (1960) Elasticity of some high density crystals. J Phys Res 65:757–766

Wang Z, Ji S (2001) Elasticity of six polycrystalline silicate garnets at pressure up to 3.0 GPa. Am Mineral 86:1209–1218

Wang H, Simmons G (1974) Elasticity of some mantle crystal structures 3. Spessartite-almandine Garnet. J Phys Res 79:2607–2613

Willmott PR, Meister D, Leake SJ, Lange M, Bergamaschi A, Böge M, Calvi M, Cancellieri C, Casati N, Cervellino A, Chen Q, David C, Flechsig U, Gozzo F, Henrich B, Jäggi-Spielmann S, Jakob B, Kalichava I, Karvinen P, Krempasky J, Lüdeke A, Lüscher R, Maag S, Quitmann C, Reinle-Schmitt ML, Schmidt T, Schmitt

B, Streun A, Vartiainen I, Vitins M, Wang X, Wullschlegera X R (2013) The materials science beamline upgrade at the Swiss light source. J Synchrotron Radiat 20:667–682. https://doi.org/10.1107/S0909049513018475

Woodland AB, Droop G, O'Neill HSC (1995) Almandine-rich Garnet from near Collobrieres, Southern France, and it's petrological significance. Eur J Mineral 7:187–194

Zhang L, Ahsbahs H, Kutoglu A, Geiger CA (1999) Single-crystal hydrostatic compression of synthetic pyrope, almandine, spessartine, grossular and andradite garnets at high pressures. Phys Chem Miner 27:52–58

Zhong X, Moulas E, Tajčmanová L (2018) Tiny timekeepers witnessing high-rate exhumation processes. Sci Rep 8:2234. https://doi.org/10.1038/s41598-018-20291-7

Zhong X, Wallis D, Kingsbery P, John T (2024) The effect of aqueous fluid on viscous relaxation of Garnet and modification of inclusion pressures after entrapment. Earth Planet Sci Lett 636:118713. https://doi.org/10.1016/j.epsl.2024.118713

Publisher's note Springer Nature remains neutral with regard to jurisdictional claims in published maps and institutional affiliations.

Springer Nature or its licensor (e.g. a society or other partner) holds exclusive rights to this article under a publishing agreement with the author(s) or other rightsholder(s); author self-archiving of the accepted manuscript version of this article is solely governed by the terms of such publishing agreement and applicable law.

Authors and Affiliations

Ross J. Angel[1] · Marta Morana[2] · Sergio Speziale[3] · Nicola P. M. Casati[4] · Alan B. Woodland[5] · Matteo Alvaro[6] · Guy L. Hovis[7] · Mario Tribaudino[8]

✉ Ross J. Angel
ross.angel@igg.cnr.it

✉ Marta Morana
marta.morana@unifi.it

✉ Sergio Speziale
speziale@gfz.de

✉ Nicola P. M. Casati
nicola.casati@psi.ch

✉ Alan B. Woodland
woodland@em.uni-frankfurt.de

✉ Matteo Alvaro
matteo.alvaro@unipv.it

✉ Guy L. Hovis
hovisguy@lafayette.edu

✉ Mario Tribaudino
mario.tribaudino@unito.it

[1] Istituto di Geoscienze e Georisorse, Consiglio Nazionale delle Ricerche, Corso Stati Uniti 4, 35127 Padova, Italy

[2] Department of Earth Sciences, University of Florence, Via G. La Pira 4, 50121 Florence, Italy

[3] GFZ Helmholtz Centre for Geosciences, D-14473 Telegrafenberg, Potsdam, Germany

[4] Paul Scherrer Institute, Forschungsstrasse 111, 5232 Villigen, Switzerland

[5] Institut für Geowissenschaften, Goethe-Universität Frankfurt, Altenhöferallee 1, 60438 Frankfurt am Main, Germany

[6] Department of Earth and Environmental Sciences, University of Pavia, Via A. Ferrata 1, 27100 Pavia, Italy

[7] Department of Geology & Environmental Geosciences, Lafayette College, Easton, PA 18042, USA

[8] Dipartimento di Scienze della Terra, Università di Torino, Via Valperga Caluso 35, I-10125 Torino, Italy